

## Geothermal Exploration in the Virunga Prospect, Northern Rwanda

Egbert Jolie

Federal Institute for Geosciences and Natural Resources (BGR), Stilleweg 2, 30159 Hannover, Germany

egbert.jolie(at)bgr.de

**Keywords:** geothermal, Rwanda, Karisimbi

### ABSTRACT

As part of a governmental policy for technical cooperation, Germany is poised to join partner countries in geothermal energy exploitation. Therefore, the Federal Institute for Geosciences and Natural Resources (BGR) on behalf of the Federal Ministry for Economic Cooperation and Development (BMZ) is carrying out the technical cooperation program GEOTHERM. As an example of the ongoing activities, results of studies carried out in the Virunga geothermal prospect in Northern Rwanda are presented.

The study area is located along the Western branch of the East African Rift System (EARS). Weak geothermal surface manifestations (e.g. hot/ cold springs with gas emanations) indicate the existence of a hydrothermal system. The aim of this study is to detect and assess potential heat sources with a multi-method approach. Remote sensing techniques, geochemical analyses, and geophysical measurements were applied in this first attempt.

Aerial photographs and satellite images were used for a high-resolution structural analysis to determine major fault zones. By performing a regional geophysical survey (Magnetotellurics, Transient Electromagnetics), an anomalous zone of low resistivities was detected in the vicinity of the Karisimbi stratovolcano, which is supported by the results of the geochemical analyses. Additional detailed geophysical investigations and gas measurements will provide insight to determine whether this anomaly is a magmatic intrusion or if the low resistivities are caused by a deep-seated fault zone.

### 1. INTRODUCTION

Traditionally, Rwanda has relied on two main sources of energy: biomass and hydropower. Biomass is the principal source of primary energy for 90 % of the population. On the other hand, imported petroleum fuels and hydropower dominate the energy supply to local industries. The country was hit particularly hard in 2004 by severe power supply shortages in the main grid due to low reservoir levels and lack of adequate plans for new generation capacity and network maintenance. Moreover, there had hardly been any investment in the energy sector for new generation capacity or in the existing network for 25 years. Low rainfall and mismanagement of reservoirs led to massive load shedding all over the country.

The Rwandan government then decided to resort to diesel based power generation temporarily to ensure a stable power supply. Unfortunately, this came at a high cost, as global oil prices rose steadily. To ensure an affordable electricity tariff, the government is currently subsidizing the energy sector by paying parts of the capacity charges for the

rented diesel generators and parts of the fuel costs. Furthermore, fuel has been exempted from import duty.

Currently, the energy portfolio in Rwanda has changed from almost entirely hydropower generated electricity to largely thermal power generation. The installed capacity of hydropower plants is approximately 27 MWe, but the available capacity at present has been lowered to 5,1 MWe as a consequence of low rainfall and insufficient refilling of the water reservoirs. To overcome the energy deficit, thermal stations were installed in 2004 and 2005 with a capacity of 29 MWe. However, these fuel-oil powered generators put a further strain on the national budget.

The total installed capacity in Rwanda is 72 MWe, but the available capacity is just above 44 MWe. This capacity satisfies slightly less than half of the national demand, and electricity is used by only 4 % of the population. At present, the electricity supply has stabilized, and unplanned power cuts rarely occur. However, the total available power is still very low, with a peak load of about 60 MWe. Only a very limited portion of the population has access to modern energy, and total connections to the electricity grid amount to about 5 % of all households. A tariff of 22 US\$cents/kWh continues to be maintained in order to cover the running costs of Reco-Rwasco (Rwanda Electricity Corporation). Clearly, this is a serious barrier in Rwanda's economic growth.

Rwanda has a large range of renewable resources that can improve its energy situation, such as solar, wind, micro hydro, geothermal energy and methane gas. At present, the priority of Rwanda's government lies on developing other indigenous energy resources in the country to meet the increasing energy demand and reduce polluting thermal stations.

The country may host medium and low enthalpy geothermal zones, but has no long history in geothermal resource exploration. It was only recently that the Rwandan Ministry of Infrastructure started to take serious steps toward exploiting this energy source. The principal objectives of the government are the evaluation of the geothermal resources in the country and the selection of sites with the highest potential for future electricity generation from these resources.

### 2. STUDY AREA

The study area is located at the border triangle between the Democratic Republic of Congo, the Republic of Uganda, and the Republic of Rwanda. The maximum WSW-ENE extension is 63 km, whereas the maximum NNW-SSE extension is 17 km. The target area covers about 600 km<sup>2</sup> and ranges from Lake Kivu in the West to Lake Ruhondo in the East, as shown in Figure 2.

Geologically, the Virunga Geothermal Prospect is located at the Western branch of the East African Rift System, which

is considered to be a developing, divergent tectonic plate boundary that divides the African Plate into two new plates called the Nubian and Somalian subplates. The rift extends 6,000 km from Zambeze river to the Red sea and splits into two main branches called the Eastern Rift Valley (Figure 1) and the Western Rift Valley. The EARS is currently in a rifting phase, which is the first step of sea opening and intrusion of alkaline magma, and apparent oceanic crust generation has begun.

The Western Rift, also called the Albertine Rift, is bordered by some of the highest mountains in Africa (Virunga Mountains, Mitumba Mountains, Ruwenzori Range) and contains the Rift Valley lakes (e.g. Lake Tanganyika - 1,470 m).

### 3. METHODS

Extensive studies were conducted by BRGM (Bureau de Recherches Géologiques et Minières) in the early 1980s at hydrothermal springs in the Western and Southern parts of the country. Secondary preliminary assessment of the two geothermal prospects (Gisenyi, Mashyuza) was carried out by Chevron in 2006.

For more detailed assessment, additional hot, warm, and mineralized springs were sampled and analyzed in 2008 by the GEOTHERM Program.

At the same time, a detailed structural analysis was carried out using satellite images and aerial photographs. Based on the results of the geochemical investigation and structural analysis, a geophysical reconnaissance survey was carried out. Subsequently, the diffuse soil degassing has been assessed for a better understanding of the system.

#### 3.1 Geochemical analysis

Water samples were collected from various sources in the study area, such as rainwater, rivers, lakes, cold springs, mineralized springs, and hot springs. During the geochemical field campaign, 24 water samples were collected to test for cations, anions, stable isotopes, strontium and tritium. The field survey also included the documentation of in-situ parameters such as pH, conductivity, and temperature.

Additional gas samples were collected from 10 sites, both for 1) analysis of the principle gas components and carbon isotopic composition and 2) helium isotopic measurements. Carbon dioxide and other reactive gas emissions were sampled from bubbling hot and cold springs using glass flasks, while helium gas emissions were sampled in sealed copper tubes. All samples were analyzed in BGR laboratories, except for tritium and helium samples, which were analyzed at the University of Bremen, Germany.

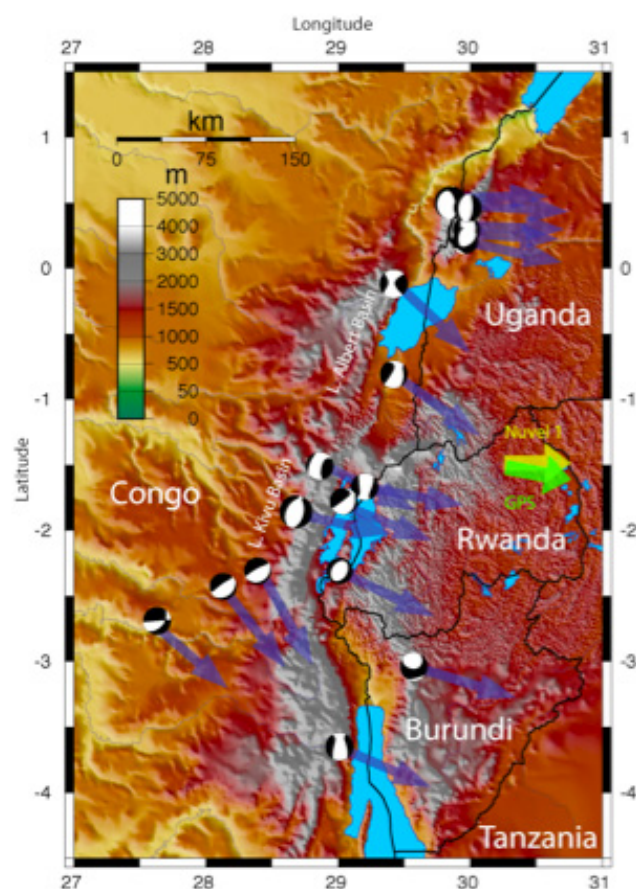


**Figure 1: Kinematics of the Western Branch of the EARS.** The yellow arrow shows NUVEL 1A (deMets et al., 1994) predicted plate motion, and the green arrow GPS present day motion (UNAVCO). The blue arrows represents slip vectors determined from the focal mechanisms (Harvard CMT). Elevation from GTOPO30 (<http://edc.usgs.gov/products/elevation/gtopo30/gtopo30.html>).

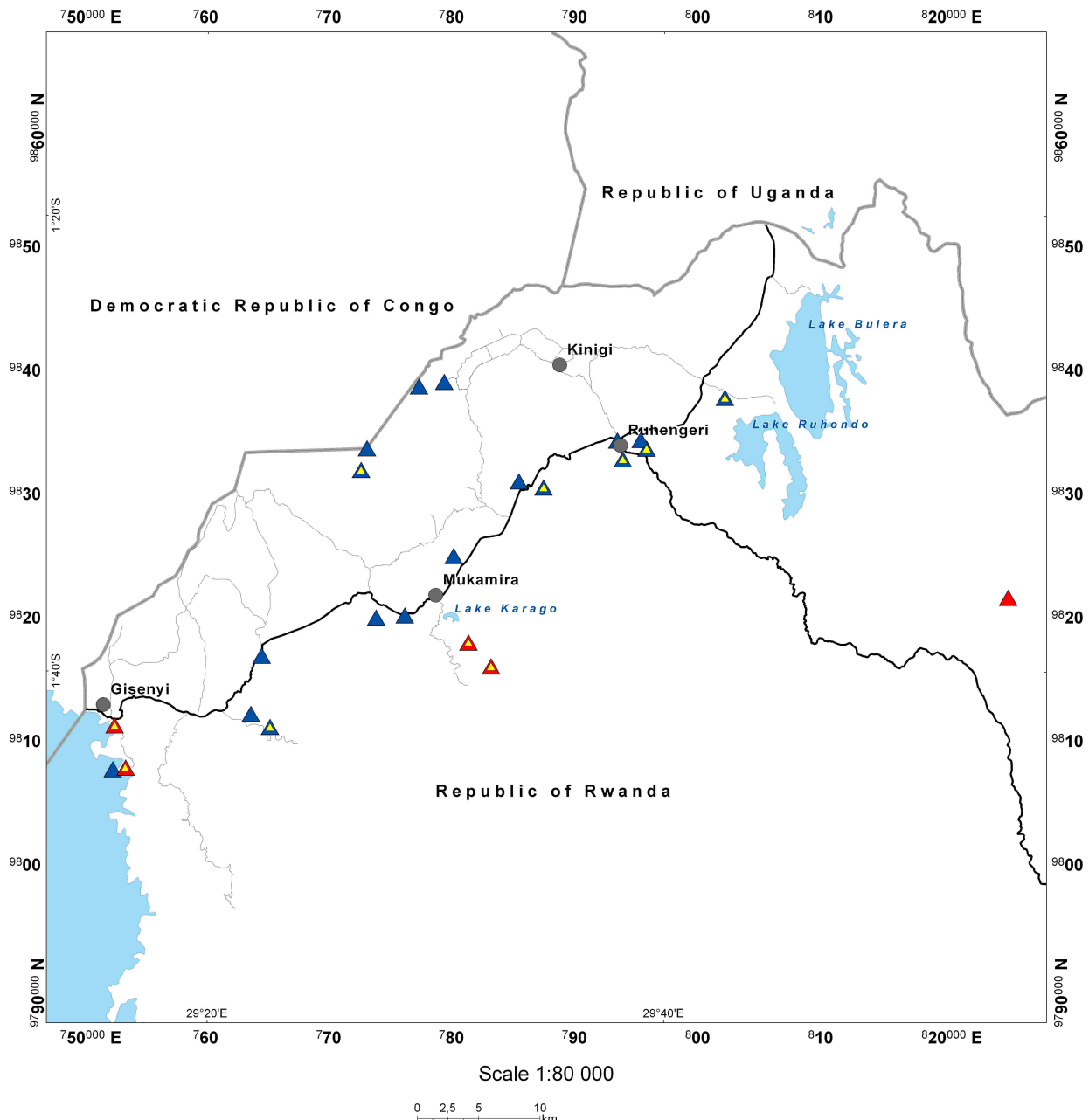


**Figure 2: Study area with sampling sites marked. Blue triangles represent cold springs, red triangles represent warm or hot springs, and yellow triangles represent gas emanations.**

### 3.2 Structural analysis

Photogrammetry has been established as the main technique to obtain precise three-dimensional measurements. It involves the use of overlapping images to recreate the original stereo geometry of each adjacent pair of images, from which precise three-dimensional measurements can be derived. Faults, lineaments and breaching angles were digitized, and their orientations were statistically analyzed.

### 3.3 Geophysical reconnaissance survey

Geothermal water has a tendency of reducing the resistivity of its host rock due to high concentrations of dissolved ions in the fluid (high salinity) and secondary alteration minerals that are formed when the thermal waters interact with the

host rock. The type of alteration minerals being formed depends on the type of the host rock and the temperature and salinity of the fluid. At temperatures lower than 220 °C, minerals such as zeolites and smectite are formed. Smectite is a clay mineral that has hydrated and loosely bound cations between the silica plates, so it is conductive and has a high cation exchange capacity. At higher temperatures, the minerals that are formed are dominantly resistive. Aside from surface manifestations such as hot springs and fumaroles, the resistivity of subsurface rocks is the most diagnostic parameter of geothermal activity that can be measured from the surface.

Magnetotellurics (MT) is a passive, geophysical surface technique that uses the horizontal components of time

variations in earth's natural electric and magnetic fields to study the electrical resistivity of the subsurface. Magnetic and electrical fields are measured in the frequency band, ranging from  $10^{-4}$  Hz to 10 kHz. High frequencies ( $> 1$  Hz) come from thunderstorm activities in the equatorial belt, while the low frequencies ( $< 1$  Hz) occur due to interaction between the solar wind and the earth's magnetic field (magnetosphere) and ionosphere.

### 3.4 Diffuse soil degassing

A total of 845 soil gas efflux and temperature measurements, 728 soil gas Radon measurements and 817 soil gas samples were performed during the gas survey, after taking into consideration the geological and structural characteristics of the study area. The average distance between each sampling site was 200 m with the aim of detecting soil gas anomalies on a relatively small scale. The elevations of the sampling sites ranged from 1.803 m asl to 3.690 m asl.

In-situ measurements of carbon dioxide and hydrogen sulphide efflux from the soil, soil temperature at 15 cm and 40 cm depth, air temperature, and radon (Rn) and thorium (Th) gas efflux were performed. Soil gas samples at each sampling site were collected for laboratory analysis of the chemical and isotopic composition of the gas.

#### 3.4.1 Soil gas sampling

Soil gas samples were collected at depths of 30-40 cm using a metallic soil probe and 20 cc hypodermic syringes, and stored in evacuated 10 cc vacutainers for the laboratory analysis of bulk composition (Hinkle et al., 1979). Soil gas concentrations were measured using a gas chromatograph. To avoid any contamination with atmospheric air, the vacutainers were previously filled with acidified water to avoid the dissolving of carbon dioxide.  $\text{CuCl}_2$  was added to the water to avoid any biological activity. During the sampling, the first 20-40  $\text{cm}^3$  of gas were withdrawn to avoid air contamination in the samples.

#### 3.4.2 Measurement of $\text{CO}_2$ and $\text{H}_2\text{S}$ efflux at the surface environment

To measure the soil carbon dioxide efflux, the closed accumulation chamber method was applied (Parkinson, K.J., 1981; Norman et al., 1997; Baubron et al., 1991; Chiodini et al., 1998). Sites of soil carbon dioxide and hydrogen sulphide efflux measurements were selected to cover most of the study area with a site spacing about 200 m. Measurements of soil  $\text{CO}_2$  and  $\text{H}_2\text{S}$  efflux were performed in-situ, using three portable soil flux meter. Each device consists of a portable non-dispersive infrared  $\text{CO}_2$  analyzer and an electrochemical  $\text{H}_2\text{S}$  sensor. The LICOR and DRAGER analyzers were interfaced to a hand size computer running the data acquisition software. To avoid the interference of water in the IR sensor, a  $\text{Mg}(\text{ClO}_4)_2$  trap was used before the gas enters the sensor.

Having placed the chamber on the ground, the circulation of the gas was forced in a closed loop between the chamber and the analyzer. In the hand size computer, the increase of both  $\text{CO}_2$  and  $\text{H}_2\text{S}$  concentrations were recorded as a function of time, allowing the operator to calculate the  $\text{CO}_2$  and  $\text{H}_2\text{S}$  efflux at each measuring site. To verify the performance and the reliability of this method, several calibration tests were performed in the laboratory, and the accuracy was estimated to be  $\pm 10\%$ . During the field work, rain and strong wind conditions were avoided.

This method enabled the calculation of the gas efflux from the initial slope of changes in concentration with time. The mathematical equations used to justify the accumulation chamber method account for the mass balance and regular volumetric geometry.

#### 3.4.3 In-situ analysis of radon ( $^{222}\text{Rn}$ ) and thorium ( $^{220}\text{Rn}$ ) activities in the soil atmosphere

Measurements of Rn activity in soil gases were performed using two SARAD RTM2010 Radon Monitors. Gas from the soil atmosphere at 40 cm depth was pumped by an internal pump (monitor) to the sensor. The RTM2100 is a universal Radon/Thoron monitor for portable and stationary applications. Its high sensitivity and alpha spectroscopic analysis result in the smallest possible response time, even at low Radon concentrations. The Thoron concentration was determined simultaneously. The instrument has additional temperature, humidity, barometric pressure and flow rate sensors.

The RTM2100 consists of a high voltage gauge with an electrostatic collection of ionized Radon daughters (generated inside the gauge) on the surface of a silicon detector. The measurement is based on alpha spectroscopy.

## 4. RESULTS

### 4.1 Geochemical analysis

Two major geochemical sampling campaigns were carried out in the study area from January to March 2008. Most of the investigated geothermal surface manifestations are situated along the Muhungwe escarpment, which represents the contact between the Accommodation Zone and the geological basement (Butare Horst), as shown in Figure 6. Springs occur up to 10 km south of the escarpment along SSE striking fault zones within the geological basement. No alteration was observed in the study area. Only five sites, surveyed in 2008, exhibited increased surface temperatures, but two of them were distant from the study area. The spring at Mashyuza (73,1 °C) near Gisenyi and the spring at Lake Karago (64,1 °C) exhibited the highest temperatures.

Fairly small outflow rates of up to 4 l/s were estimated in the sampled springs. Some springs showed relatively weak gas emanations. No fumarolic manifestations were found, however, huge areas were inaccessible for the field exploration, particularly in the Volcanoes National Park. Thus, additional springs may exist. It is also assumed that further hot springs are located at the bottom of Lake Kivu in the center of the Albert Rift. This assumption is supported by the fact that enormous amounts of carbon dioxide and methane are dissolved in the water and sediments of the lake, caused by both volcanic and bacterial activity.

BRGM (Fabriol and Verzier, 1983; Ranchon and Demange, 1983) carried out an extensive study of the geothermal resources and found potential due to good permeability, abundant rainfall, and the presence of potential heat sources, especially in the Southwest of the Karisimbi volcano.

Computations of various geothermometer temperatures (Arnorsson et al., 1983; Fournier, 1977; Fournier and Potter, 1982) have been carried out using the WATCH code (Arnorsson et al., 1982; Bjarnason, 1994). Most of the samples did not seem to be at equilibrium. They have been relatively cold under conditions, in which it takes a very

long time to reach equilibrium between minerals and water. Several were rich in carbonates, and this may have distorted the results further. Thus, cation geothermometers were considered unreliable, with the exception of the silica geothermometer, which should be effective for at least the hotter samples. The main criteria for disequilibrium are a low Na/K ratio (< 5) and a high magnesium concentration (> 30 ppm).

To establish the equilibrium state a Na-K-Mg diagram (Giggenbach, 1988) was compiled for the samples from the warm/ hot springs. Two samples that had shown possible geothermal characteristics were included in the Na-K-Mg plot. The results in Figure 4 show that all samples are high in magnesium. The sample of Bitagata, Iriba and Mpatsi plot as immature waters, and the other samples plot close to the curve, which separates equilibrated from immature waters.

When estimating subsurface temperatures, it was considered that the springs in these locations emanate from the old basement rock and were more likely to have reached equilibrium with quartz than with chalcedony. Using these criteria, possible temperature ranges were obtained for six samples, all of which indicated geothermal character (four were taken from warm and hot springs, and two were taken from cold springs). The sample from Bitagata could not be assessed in the same way and is either not much hotter than the source sampled or heavily mixed with ground water. The probable temperature ranges for the six samples are shown in Figure 3.

#### 4.2 Structural analysis

998 Lineaments, 114 cone breachings, and 312 major cone axes were digitized and analyzed. The linearized river system was also studied. A map of the lineaments is shown in Figure 5. The lineament trends are largely dominated by NS structures related to Proterozoic mobile belts. Two secondary directions (ENE and WNW) were also observed. Three sub-areas were defined based on their geological settings. LD1 is located in the accommodation zone, which is filled with quaternary lavas. LD2 is a horst structure (Butare Horst), composed of Proterozoic, mylonitised granitic and phyllitic complexes. LD3 represents a series of folded Precambrian metasediments.

(A) LD1 is marked by two major trends centered on N30-50 and N150-170.

(B) LD2 is marked by two major trends centered on N10-20 and N130-140.

(C) LD3 is marked by two major trends centered on N0 and N60-70.

Both N-S and WSW-ENE lineament groups are related to Proterozoic orogenes. Both trends were reactivated as normal faults by the Miocene to Quaternary deformation. The NNW-SSE trend is related to Tertiary (e.g. Kamatembe) reactivated structures parallel to the Tanganyika-Rukwa-Malawi Zone, a major Transafrican Precambrian shear zone.

Location	Likely temperature range °C
Mbonyebyombi	110-130
Mpatsi	130-150
Karago	120-140
Gisenyi	105-130
Iriba	110-120
Nyakageni	110-140

**Figure 3: Assumed subsurface temperatures, calculated by silica geothermometer**

## Na/1000

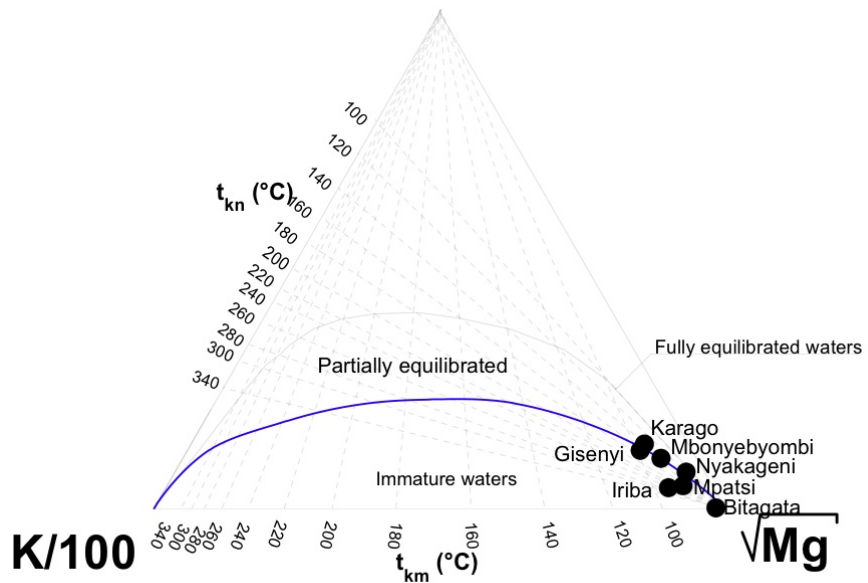


Figure 4: Na-K-Mg diagram

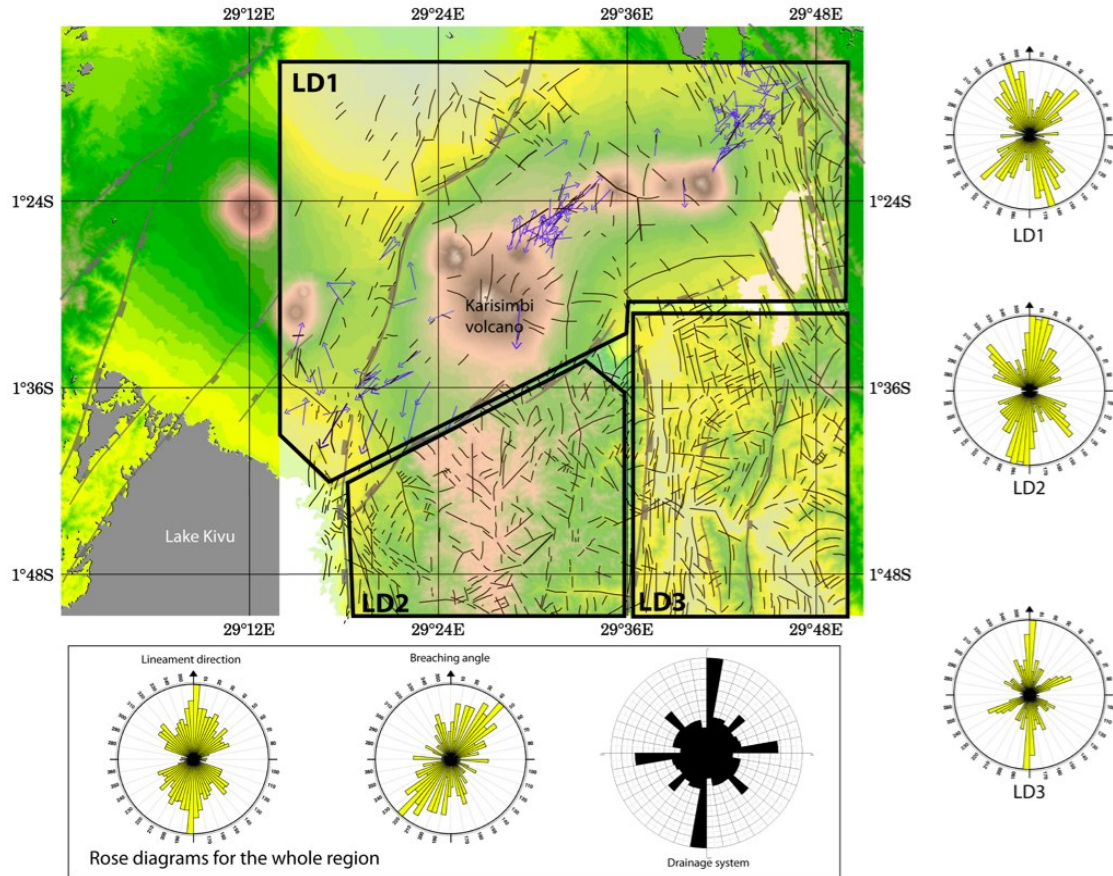
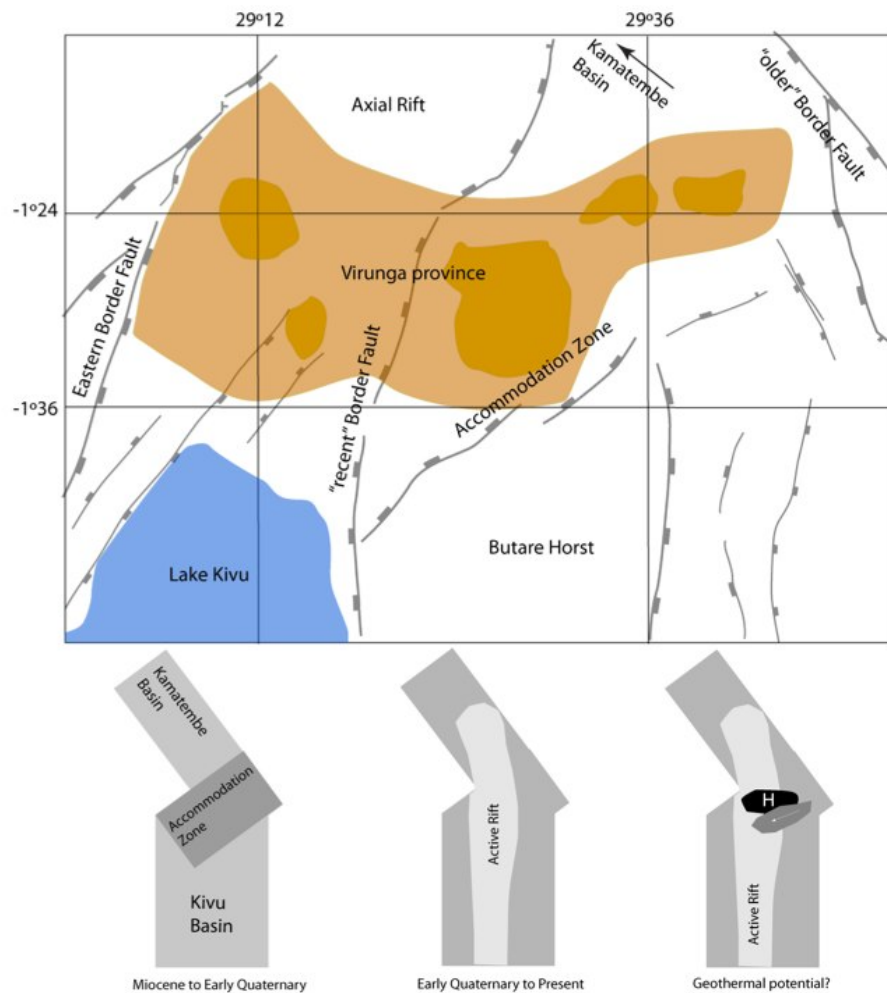


Figure 5: Lineaments and fault statistics



**Figure 6: Structural sketch map. Bottom: evolution of the rift system and potential geothermal zone (H: heat source; white arrow: large water flow; dark grey area: the location where heat proximity, intense faulting, and water presence are highest.**

#### 4.3 Geophysical analysis

The MT resistivity survey showed that the granitic basement rocks in the Gisenyi-Ruhengeri area generally have very high resistivities. Lava materials from the quaternary volcanoes (Karisimbi, Bisoke, Sabyinyo, Gahinga, Muhabura) cover a great part of the study area. These lavas are relatively young and less altered, and thereby exhibit high resistivity at the surface to depths of a few hundred meters.

Isolated lower grounds in the study area contain hydrated sediments (e.g. silt, sand) and exhibit low resistivity values at the surface. Other areas, including the Ndorwa hot spring near Lake Karago and the Gisenyi hot springs at the shores of Lake Kivu, where hydrothermal fluids find their way to the surface through fractures, displayed moderately low resistivity at the surface. It is assumed that this is caused by alteration of the rocks in these fractures.

The most prominent anomaly was found SW of Karisimbi (Figure 7), along the Northern boundary of the Butare Horst. Sparse MT data points hindered the full delineation of the boundaries and depths of these anomalies. So far, the cause of this low resistivity anomaly cannot be stated with

certainty. A possible explanation for this is the presence of conductive alteration minerals in the fractures of the resistive basement rock and/or magmatic intrusions in deeper zones.

#### 4.3 Diffuse soil degassing

Most of the diffuse degassing studies performed at volcanic areas focus on the measurement of the CO<sub>2</sub> efflux, since CO<sub>2</sub> is the most abundant species among the volcanic gases besides water. Recently published works in international journals (Chiodini et al., 1996; Pérez et al., 1996a; Hernández et al., 1998) have demonstrated the link between the CO<sub>2</sub> efflux, the volcanic-structural features, and the eruption dynamics.

During the field work, measurements of CO<sub>2</sub> efflux at the surface environment were performed by means of the accumulation chamber method. The CO<sub>2</sub> efflux values ranged from below detection limit (< 20 g/m<sup>2</sup>/d) to a maximum value of 3.244 g/m<sup>2</sup>/d, measured at the Karago hot spring. From these data, it was possible to estimate that across the study area a total of 6.778 t/d of CO<sub>2</sub> are emitted to the atmosphere.

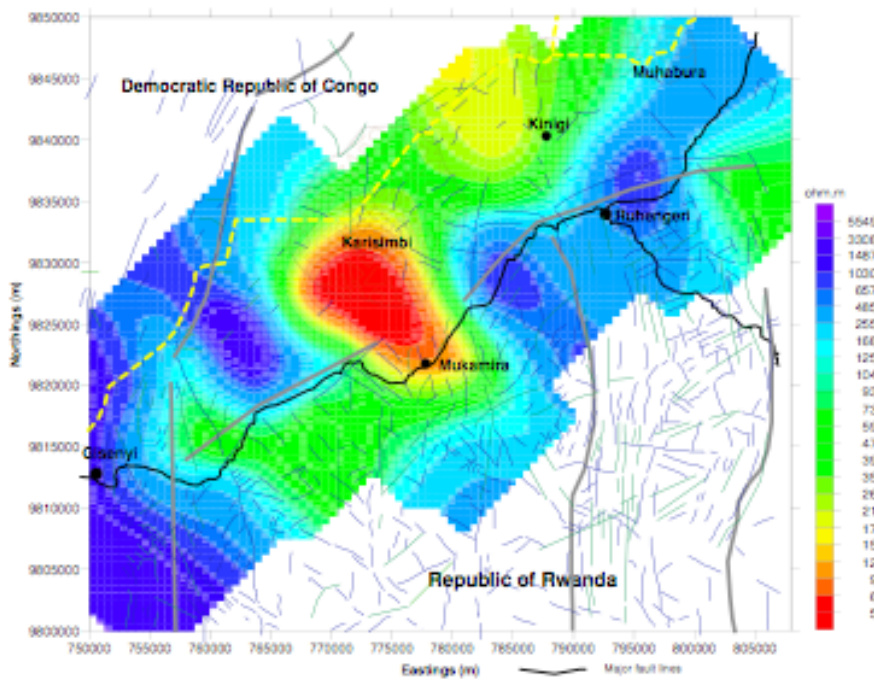


Figure 7: Resistivity distribution in 6000 m bsl, derived from MT measurements.

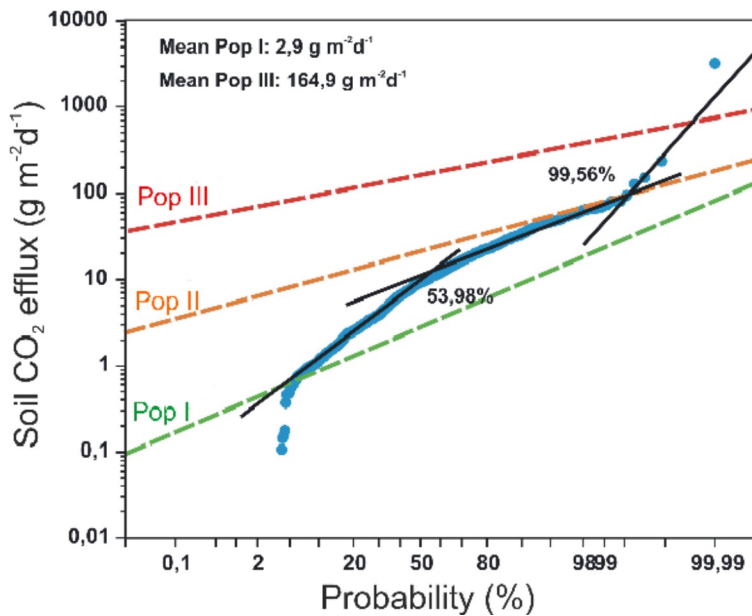
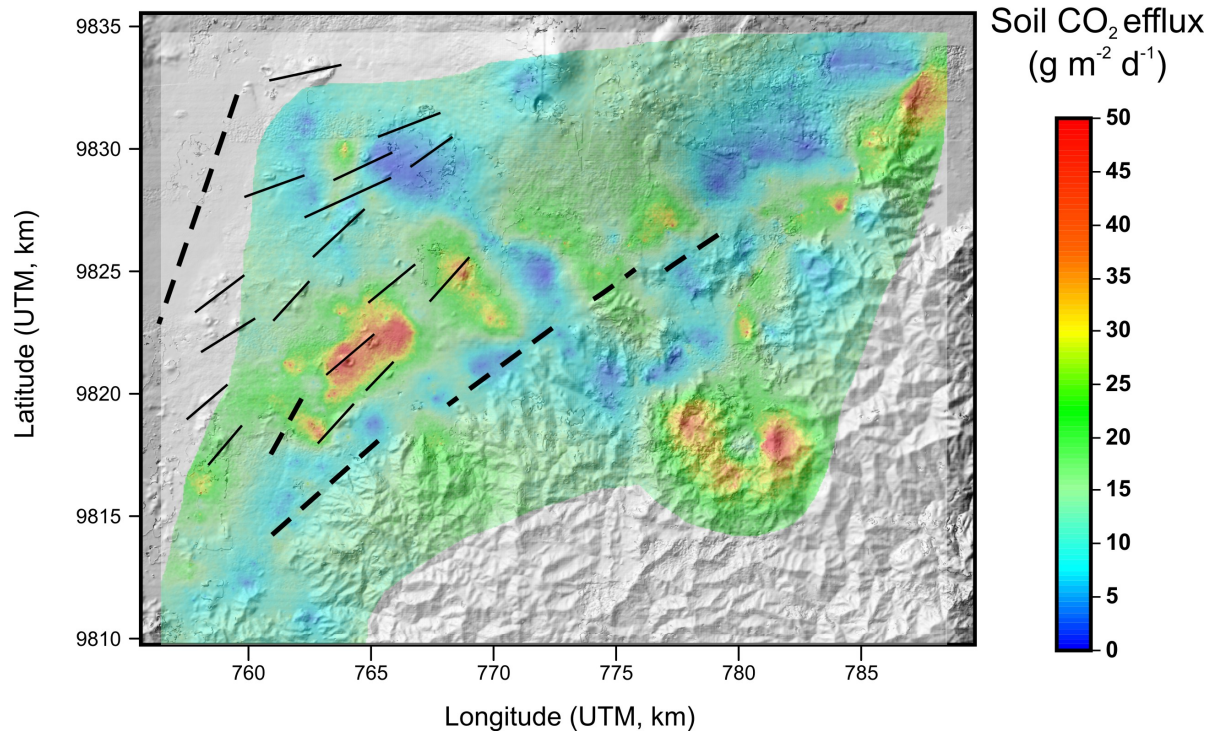


Figure 8: Statistical graphical analysis of carbon dioxide efflux data.

Sinclair statistical graphical analysis was performed to distinguish different geochemical populations of the  $\text{CO}_2$  efflux data. As can be seen in Figure 8, three overlapping geochemical populations were distinguished in this analysis: (1) Population I or background population, representing 53,98 % of the total data with a mean value of  $2,9 \text{ g/m}^2/\text{d}$ ; (2) Population II or mix population, representing 45,58 % of the total data with a mean value of  $21,0 \text{ g/m}^2/\text{d}$ ; and (3) Population III or peak population, representing 0,44 % of the total data with a mean value of  $164,9 \text{ g/m}^2/\text{d}$ .

The  $\text{CO}_2$  emissions corresponding to the background population are related to a biogenic origin (soil respiration, degradation of organic matter, etc.). Most of the study area exhibited background  $\text{CO}_2$  efflux values.

A spatial distribution map was generated of the  $\text{CO}_2$  efflux data using the SGs algorithm provided by GSLIB software. The main volcanic-structural features of the area were included in the distribution map. A SW-NE alignment of anomalous  $\text{CO}_2$  efflux values was observed in conjunction with a zone located in the SW part of



**Figure 9: Diffuse soil carbon dioxide emissions**

the study area surrounding the Karago hot spring, as shown in Fig. 9. Diffuse  $\text{H}_2\text{S}$  efflux was also measured at all points. However, only two places exhibited efflux values above the detection limit of the instrument ( $0.01 \text{ mg/m}^2/\text{d}$ ). These values ( $0.68 \text{ mg/m}^2/\text{d}$  and  $0.05 \text{ mg/m}^2/\text{d}$ ) were measured around the hot springs at Lake Karago.

## 5. CONCLUSION

Water and gas samples were analyzed for cations, anions, stable isotopes, strontium and tritium. Good permeability was generally indicated, and subsurface temperatures in excess of  $100^\circ\text{C}$  can be expected at six locations. Data suggest that four of the springs (Mbonyebyombi, Mpatsi, Karago and Gisenyi) are located atop a geothermal system, in which temperatures may exceed  $100^\circ\text{C}$ . Two other locations (Iriba and Nyakageni) also exhibited geothermal character and possibly similar temperatures. The composition of the water from the Bitagata warm spring suggested a lower source temperature. All appeared to discharge where permeability is likely to be considerable. Further indications suggest that Gisenyi and Karago are probably the most promising locations. None of these locations suggested high temperature geothermal systems, but they might be suitable for the production of electricity using binary power plants.

Additional detailed geophysical measurements with a smaller spacing should be performed to better understand the characteristics of these systems.

## REFERENCES

Arnórsson, S., Gunnlaugsson, E. and Svavarsson, H. (1983). The chemistry of geothermal waters in Iceland I. Chemical geothermometry in geothermal investigations. *Geochim. Cosmochim. Acta*, 47, 567–577.

Arnórsson, S., Sigurðsson, S. and Svavarsson, H. (1982). The chemistry of geothermal waters in Iceland III. Calculation of aqueous speciation from  $0^\circ\text{C}$  to  $370^\circ\text{C}$ . *Geochim. Cosmochim. Acta*, 46, 1513–1532.

Baubron, J., Mathieu, R., Miele, G. (1991): Measurement of gas flow from soils in volcanic areas: the accumulation method. Napoli'91 International Conference on active volcanoes and Risk Mitigation. *Abstract*., 27 August-1 September 1991, Napoli, Italy.

Bjarnason, J. O. (1994). The speciation program WATCH, version 2.0. *Orkustofnun*.

Chevron, 2006. Preliminary Assessment of Rwanda's Geothermal Energy Development Potential.

Chioldini, G., Cioci, R., Guidi, M., Raco, B., Marini, M. (1998): Soil Flux measurements in volcanic and geothermal areas. *Appl. Geochem.*, 13, (5), 543-552.

Chioldini, G., Frondini, F., Raco, B. (1996) : Diffuse emission of  $\text{CO}_2$  from the Fossa crater, Vulcano Island (Italy). *Bull. Vulcanol.*, 48, 41-50.

DeMets, C., Gordon, R.G., Argus, D.F. and Stein, S., 1994. Effect of recent revisions to the geomagnetic reversal time scale on estimates of current plate motions. *Geophysical Research Letters* 21, 2191–2194.

Fabriol, R.; Verzier, P. (BRGM) 1983. Reconnaissance Géothermique de la République du Rwanda, Rapport Hydrogeochimique.

Fournier, R. O. (1977). Chemical geothermometers and mixing models for geothermal systems, *Geothermics*, 5, 41–50.

Fournier, R. O. and Potter, R. W. II (1982). A revised and expanded silica (quartz) geothermometer. *Geoth. Resourc. Counc. Bull.*, 11[U+2010]10, 3–12.

Giggenbach, W.F. (1988). Geothermal solute equilibria. Derivation of  $\text{Na}[\text{U}+2010]\text{K}[\text{U}+2010]\text{Mg}[\text{U}+2010]\text{Ca}$  geoindicators. *Geochim. Cosmochim. Acta*, 52, 2749–2765.

Hernández, P., Pérez, N., Salazar, J., Nakai, S., Notsu, K., Wakita, H. (1998): Diffuse emission of carbon dioxide, methane, and helium-3 from Teide volcano, Tenerife, Canary Islands. *Geophys. Res. Lett.*, 25, 3.311-3.314.

Hinkle, M.E., Kilburn, J.E.: The use of vacutainer tubes for collection of soil gas samples for helium analysis, U.S. Geological Survey Open-File Report 79,1441 (1979).

Norman, J.M., Kucharik, C.J., Gower, S.T., Baldocchi, D.D., Crill, P.M., Rayment, M., Savage, K., Striegl, R.G., (1997): A comparison of six methods for measuring soil-interface carbon dioxide fluxes. *J. Geophys. Res.* 102, 28771-28777.

Parkinson, K. (1981): An improved method for measuring soil respiration in the field. *J. Applied Ecology* 18, 221-228.

Pérez, N., Wakita, H., Lolok, D., Patia, H., Talai, B., McKee, C. (1996a): Anomalous soil gas  $\text{CO}_2$  concentrations and relation to seismic activity at Rabaul Caldera, Papua New Guinea. *Geogaceta* 20, 1.000-1.003.

Ranchon, J. Ph. and Demange, J., 1983. Reconnaissance geothermique de la Republique du Rwanda, Rapport geovolcanologique, BRGM, Paris.